ARCHIVES OF MECHANICS
Arch. Mech. **72** (5), 445–464, 2020, DOI: 10.24423/aom.3590

Misfit dislocation in a precipitate/matrix interface of any orientation relative to the matrix free-surface

J. COLIN

Institut Pprime, CNRS-Université de Poitiers-ISAE-ENSMA, UPR 3346, TSA 41123, 86073 Poitiers Cedex 9, France, e-mail: jerome.colin@univ-poitiers.fr

The presence of an edge dislocation in a surface of a two-dimensional precipitate of square shape embedded in a semi-infinite matrix has been discussed when the precipitate is submitted to misfit strain due to the lattice mismatch between the two phases. Considering any orientation of the precipitate relative to the matrix free-surface, the total force applying on the dislocation has been analytically calculated and its equilibrium position has been determined. The conjugated effects of the precipitate misorientation, of the lattice mismatch and of the precipitate/matrix distance have been finally characterized. A shifting effect on this equilibrium position has been analyzed.

Key words: dislocations, linear elasticity, micro-mechanics, modelling.

1. Introduction

The mechanical properties of multiphase and multilayered materials have been extensively studied in different fields of research among which one can cite solid mechanics, materials science and metallurgy or engineering. Indeed, the control of the deformation, ageing and deterioration of such materials is of paramount importance because of their numerous applications in aeronautic, nano-electronics and nano-optics for example. In case of single crystal superalloys used for turbine blades, it is now well-admitted that the creep deformation regime consisting in low stress and high temperature is characterized by the development of networks of dislocations in the interfaces between the cuboidal γ' precipitates and the γ matrix. Using the discrete dislocation dynamics (DDD) model, the effects of dislocation interaction and misfit stress have been numerically characterized on the motion of the interfacial dislocations and dynamic recovery [1]. Still at high temperature, the creep behavior of rafted [001] oriented AM1 Ni-based single crystal superalloys has been also experimentally investigated during in-situ creep tests on synchrotrons [2]. The interaction between the plastic stress and dislocations in the γ phase has been thus characterized under variable applied stress. Focusing on the early stages of creep for Ni-based superalloys, where the dislocations are confined in the γ channel, DDD

simulations have also shown that in the low-stress regime, a network of dislocations develops near the corners of the γ' precipitates [3]. In the high stress regime, the dislocations are squeezed into the γ channels and dislocation segments are deposited at the γ/γ' interfaces. Likewise, considering the misfit stress, the stress due to the dislocations and the external stress, the glide and climb forces on γ-channel dislocations have been calculated [4]. In particular, it has been found that the dislocation spacing corresponds to the one experimentally observed after high temperature and low stress creep. Using a three-dimensional level set dislocation dynamics method, the degree of coherency of the interface between a spherical particle and its infinite-size matrix has been also characterized when matrix dislocations are interacting with the precipitate [5]. Likewise, in the framework of atomistic-based models, the interaction between the moving dislocations in the matrix channels and the interface misfit dislocations has been studied in case of Ni-based single crystal superalloys and the effects of the type and position of the moving dislocations on the critical bowing stress for the (moving) dislocations have been determined [6].

In case of core-shell nanowires with potential applications in optoelectronics, a number of studies have also focused on the determination of the different critical parameters for the formation of defects such as straight edge dislocations [7], screw dislocations [8–10] and dislocation loops [7, 11–14]. Likewise, the possibility of formation of circular dislocation loops in bulk [15, 16] and hollow [17] core-shell nanoparticles has been investigated. When an edge dislocation is embedded in the shell of the core-shell structure, non-classical effects such as stress oscillations along the surfaces for negative surface/interface elastic moduli have been characterized on the elastic behavior of the dislocation in the framework of the surface/interface elasticity theory [18]. When the edge dislocation is lying in the core of the core-shell structure embedded in an infinite-size matrix, the interface effects have been also studied and the dislocation positions have been determined [19]. Likewise, the non-classical surface/interface effects have been investigated on the critical conditions for the formation of edge misfit dislocations, these effects being found to be significant for fine cores smaller than 20 interatomic distances [20]. The surface stress effects have been also discussed for an edge [21] and a screw [22] dislocation embedded in the wall of a multi-walled nanotube.

For a nanowire with a rectangular cross-section embedded in a semi-infinite matrix, the formation of loops, semi-loops and dipoles of misfit dislocations in the precipitate/matrix interface has been recently theoretically investigated from an energy variation calculation [23] and the geometric parameters for which the dislocation formation is energetically favorable have been identified. Likewise, when the misfitting nanowire of the form of a long parallelepiped is embedded in a nanolayer, the stress relaxation due to the introduction of a dipole of

edge misfit dislocations in the interfaces of the precipitate perpendicular to the two free-surfaces of the layers has been studied [24]. More specifically, calculating the energy variation resulting from the introduction of this dipole from one free-surface to the interfaces, the equilibrium positions of the dislocations and the corresponding energy barriers have been calculated. Finally, it can be noticed that when two square-shaped precipitates are located near their matrix free-surface, the formation of two misfit edge dislocations gliding in two consecutive interfaces between the matrix and two neighboring precipitates has already been considered and the different equilibrium positions have been characterized [25].

In this paper, the possibility of introduction of a misfit dislocation in an interface between a square-shaped precipitate and its semi-infinite matrix has been theoretically investigated when the precipitate is tilted relative to the matrix free-surface. The influence of the orientation angle of the precipitate relative to the matrix free-surface has been discussed on the stable equilibrium position of the dislocation as well as the effects of the misfit strain and the effects of the distance of the precipitate from the free-surface.

2. Modeling and discussion

A two-dimensional square shaped precipitate (ABCD) of side L is embedded in a semi-infinite matrix (see Fig. 1 for axes). It is tilted relative to the horizon-

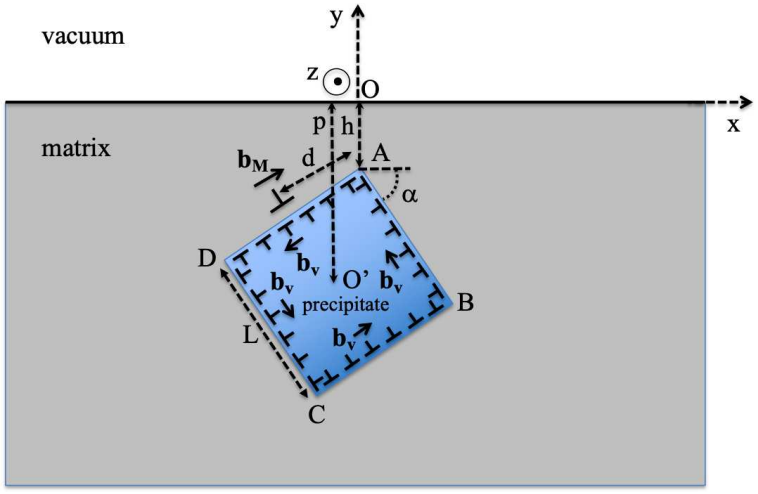

FIG. 1. Schematic in the (Oxy) plane of a square shaped precipitate embedded in a semi-infinite matrix. The position of the precipitate center from the surface is labelled p, its side L and tilt angle α. A misfit dislocation of Burgers vector $\mathbf{b}_M$ is lying in the (DA) interface between the precipitate and the matrix, at a distance d from the corner A.

tal axis of an angle α, and the distances of its center O' and corner A from the free-surface are labelled p and h, respectively, with $h = p - \frac{L}{2}\big(\cos\alpha + \sin\alpha\big)$. The shear modulus μ and Poisson's ratio ν are assumed to be equal in both matrix and inclusion phases. Despite the fact that the elastic coefficients are usually heterogeneous in superalloys [26], it is believed that the present analytical analysis with homogeneous elastic coefficients should give some insights into the effects of the matrix free-surface and the precipitate tilt angle on the misfit dislocation positions [3]. Due to the lattice mismatch $\delta a = a_* - a$ at the precipitate-matrix interfaces, a misfit strain develops in the biphase solid, with a_* and a the lattice parameters of the precipitate and the matrix, respectively [27]. To determine the stress field $\bar{\bar{\sigma}}_M$ resulting from the coherency of both lattices at the interfaces, the formalism of distributions of virtual dislocations of the infinitesimal Burgers vector has been used [28, 29], in the framework of the linear and isotropic elasticity theory [27, 30]. To do so, one row of virtual edge dislocations has been introduced on each of the four interfaces of the inclusion. The first step of this work has been to determine the stress field of one virtual dislocation of the Burgers vector $\mathbf{b}_v = (b_x^v, b_y^v)$ located at (x_v, y_v) near the free-surface, with $y_v < 0$ and $|\mathbf{b}_v| = \delta a$. The problem of the determination of the stress field in the neighborhood of the free-surface is well-known [28] and can be solved considering two dislocations, one of the Burgers vector $(b_x^v, 0)$ and one of the Burgers vector $(0, b_y^v)$, both at (x_v, y_v), using Airy's function formalism [30]. For the first dislocation of the Burgers vector $(b_x^v, 0)$, the problem has been solved considering Airy's function of an edge dislocation embedded in an infinite-size medium $\phi^0_{b_x}(x - x_v, y - y_v)$, corresponding Airy's function for its image dislocation with respect to the free-surface located at $(x_v, -y_v)$ and of Burgers vector $(-b_x^v, 0)$, and a supplementary term characterized by the Airy's function $\phi^{sup}_{b_x}(x, y)$. Airy's function $\phi_{b_x^v}$ finally writes [28]:

$$\phi_{b_x^v}(x, x_v, y, y_v) = \phi^0_{b_x^v}(x - x_v, y - y_v) - \phi^0_{b_x^v}(x - x_v, y + y_v) + \phi^{sup}_{b_x^v}(x, y), \tag{2.1}$$

with

$$\phi^0_{b_x^v}(x, y) = -\frac{\mu b_x^v}{2\pi(1-\nu)}\frac{y}{2}\ln\big[x^2 + y^2\big], \tag{2.2}$$

$$\phi^{sup}_{b_x^v}(x, y) = -\frac{\mu b_x^v}{\pi(1-\nu)}\bigg(-\frac{y_v y(y + y_v)}{(x - x_v)^2 + (y + y_v)^2} + \frac{y_v}{2}\ln\big[(x - x_v)^2 + (y + y_v)^2\big]\bigg). \tag{2.3}$$

For the dislocation of the Burgers vector $(0, b_y^v)$, an equivalent procedure has

been used and the corresponding Airy's function ϕ_{b_y} has been found to be [28]:

$$\begin{aligned}(2.4)\qquad \phi_{b_y^v}(x,x_v,y,y_v) = \frac{\mu b_y^v}{2\pi(1-\nu)}\Bigg(&\frac{x-x_v}{2}\ln\big[(x-x_v)^2+(y-y_v)^2\big]\\ &-\frac{x-x_v}{2}\ln\big[(x-x_v)^2+(y+y_v)^2\big]\\ &+\frac{2y_v y(x-x_v)}{(x-x_v)^2+(y+y_v)^2}\Bigg),\end{aligned}$$

where the first term of the right-end side of the above Eq. (2.4) corresponds to the self-term of the dislocation in an infinite-size media, the second one to its image dislocation and the third one to the supplementary term. Finally, the complete Airy's function for the dislocation of the Burgers vector (b_x^v, b_y^v) is given by:

$$(2.5)\qquad \phi_{\mathbf{b}_v}(x,x_v,y,y_v) = \phi_{b_x^v}(x,x_v,y,y_v) + \phi_{b_y^v}(x,x_v,y,y_v),$$

the stress components being derived as [30]:

$$(2.6)\qquad \sigma_{xx}^{\mathbf{b}_v}(x,x_v,y,y_v) = \frac{\partial^2}{\partial y^2}\phi_{\mathbf{b}_v}(x,x_v,y,y_v),$$

$$(2.7)\qquad \sigma_{xy}^{\mathbf{b}_v}(x,x_v,y,y_v) = -\frac{\partial^2}{\partial x\partial y}\phi_{\mathbf{b}_v}(x,x_v,y,y_v),$$

$$(2.8)\qquad \sigma_{yy}^{\mathbf{b}_v}(x,x_v,y,y_v) = \frac{\partial^2}{\partial x^2}\phi_{\mathbf{b}_v}(x,x_v,y,y,y_v).$$

Once the stress field of a virtual dislocation is known, the contribution to the misfit stress of each of the four rows located at the matrix/precipitate interfaces can be determined by summing up all the contributions of each virtual dislocation of the corresponding row. For example, taking $b_x^v = b_M \sin\alpha$ and $b_y^v = b_M \cos\alpha$, the Airy's function $\phi_M^{(CB)}$ associated with the dislocation row located on the side (CB) is defined as [28, 29]:

$$(2.9)\qquad \phi_M^{(CB)}(x,y) = \int\limits_{l(\cos\alpha-\sin\alpha)}^{l\cos\alpha} \phi_{\mathbf{b}_v}(x,x_v,y,x_v/\tan\alpha - h - l/\sin\alpha)\,\frac{dx_v}{a\sin\alpha}.$$

The other Airy's functions $\phi_M^{(DA)}$, $\phi_M^{(DC)}$ and $\phi_M^{(AB)}$ have been calculated for the sides (DA), (DC) and (AB), respectively, using equivalent formulas to the one displayed in Eq. (2.9) (see Appendix). Finally, the complete Airy's function ϕ_M characterizing the misfit stress tensor $\bar{\bar{\sigma}}_M$ can be obtained by summing up the contributions of the four rows:

$$\phi_M(x,y) = \phi_M^{(CB)}(x,y) + \phi_M^{(DA)}(x,y) + \phi_M^{(DC)}(x,y) + \phi_M^{(AB)}(x,y),$$

the stress component formulas being given in the Appendix. Once the stress field resulting from the misfit is known, its effect on an edge dislocation introduced in one interface of the precipitate to release this misfit stress can be considered from the study of the (PK) Peach–Koehler force [31]. More specifically, an edge misfit dislocation of the Burgers vector $\mathbf{b}_M = (b_M \sin\alpha, b_M \cos\alpha)$ is introduced in the (DA) interface (chosen without loss of generality) which has been slightly shifted of a quantity $\mathbf{b}_M$ into the matrix to avoid the region at the precipitate corner where the misfit stress field may diverge. Its position is thus given by $(x_M = -d\sin\alpha - b_M\cos\alpha, y_M = -h - d\cos\alpha + b_M\sin\alpha)$, where d is the distance of the dislocation from the corner A, with $d > 0$. Assuming $0 \leq \alpha \leq \pi/2$ in the present work, it is underlined that an equivalent analysis would apply to the (AB) interface. The problem of the dislocation lying in the (DC) or (CB) interface is not studied in this paper, since these interfaces are farther from the free-surface than the (DA) and (AB) interfaces and the surface effect on the dislocation position is thus assumed to be weaker. This PK force per unit length on the dislocation of the Burgers vector $\mathbf{b}_M$ due to the misfit stress $\bar{\bar{\sigma}}_M$ generated by the precipitate is defined as [31]:

$$\mathbf{F}_{PK}^M = \bar{\bar{\sigma}}_M \mathbf{b}_M \wedge \zeta, \tag{2.10}$$

with ζ the unit line vector of the dislocation along (Oz) axis. Considering the gliding part of the PK force along $\mathbf{u} = (\sin\alpha, \cos\alpha)$ direction, it yields:

$$\begin{aligned} F_{\mathbf{u}}^M(h,d,\alpha) &= \mathbf{F}_{PK}^M \mathbf{u} \\ &= -b_M \cos 2\alpha\, \sigma_{xy}^M(x_M, y_M) \\ &\quad + \frac{b_M}{2} \sin 2\alpha \left(\sigma_{yy}^M(x_M, y_M) - \sigma_{xx}^M(x_M, y_M)\right) \\ &= \frac{\mu b_M \delta a}{2\pi(1-\nu)} \Lambda(h,d,\alpha) \end{aligned} \tag{2.11}$$

where the analytical expression of the Λ function versus d, h and α which can be derived from Eqs. (4.13) and (4.14) defined in the Appendix is not displayed in this paper for the sake of compactness. Likewise, the force $\mathbf{F}_{PK}^S$ due to the free-surface of the matrix on the edge dislocation has been considered. The expression of this force is well-known [28] and has been calculated from the stress field of the dislocation whose Airy's function is equivalent to the one displayed in Eq. (2.5). Omitting the self-term of the dislocation corresponding to the stress field in the infinite-size medium and using an equivalent expression to the one displayed in Eq. (2.10), the PK force per unit length in the gliding plane due to the stress relaxation near the free-surface has been found to be [28]:

$$F_{\mathbf{u}}^S(\tilde{h}, \tilde{d}, \alpha) = \frac{\mu b_M^2}{4\pi(1-\nu)} \frac{\cos\alpha}{h + d\cos\alpha - b_M \sin\alpha}. \tag{2.12}$$

Assuming without loss of generality that $b_M = a$ and introducing the dimensionless parameters $\tilde{d} = d/a$, $\tilde{h} = h/a$ and $\tilde{L} = L/a$, the dimensionless total force has been then written as:

$$\tilde{F}^t_{\mathbf{u}}(\tilde{h},\tilde{d},\alpha) = \frac{F^M_{\mathbf{u}}(\tilde{h},\tilde{d},\alpha) + F^S_{\mathbf{u}}(\tilde{h},\tilde{d},\alpha)}{F_0} = \frac{\cos\alpha}{2\big(\tilde{h}+\tilde{d}\cos\alpha-\sin\alpha\big)} + \frac{\delta a}{a}\Lambda(\tilde{h},\tilde{d},\alpha), \tag{2.13}$$

with $F_0 = \mu b_M/\big[2\pi(1-\nu)\big]$. It is emphasized at this point that the study of the $\tilde{F}^t_{\mathbf{u}}$ variations (and zeros) will only give relevant information on the equilibrium positions (stable or unstable) of the dislocation, the study of the nucleation mechanism (from the free-surface or the interface), the determination of the energy barrier and energy gain for each mechanism would require an energy-based analysis that is beyond the scope of the present work. In Figs. 2, the reduced force $\tilde{F}^t_{\mathbf{u}}$ has been plotted versus the distance $\tilde{d}$ of the misfit dislocation from the corner A, with $\tilde{L} = 200$, this value of $\tilde{L}$ being considered as constant in the following (except for Fig. 7). Taking $\alpha = \pi/4$ and $\tilde{p} = 300$, it is found in Fig. 2a that there exists for the dislocation a stable equilibrium position $\tilde{d}_{eq}$ from corner A, i.e. $\tilde{F}^t_{\mathbf{u}} < 0$ for $\tilde{d} < \tilde{d}_{eq}$ and $\tilde{F}^t_{\mathbf{u}} > 0$ for $\tilde{d} > \tilde{d}_{eq}$, this distance $\tilde{d}_{eq}$ increasing with $\delta a/a$. Likewise, taking $\delta a/a = 0.01$ and $\tilde{p} = 300$ in Fig. 2b, it is observed that the stable equilibrium position also depends in a nontrivial way on the orientation angle α of the precipitate, the surface force in the gliding plane going to zero when $\alpha = \pi/2$ and the equilibrium position being thus the middle of the precipitate side. In Fig. 2c, it is finally observed that as the distance $\tilde{p}$ of the precipitate from the free-surface of the matrix decreases from $\tilde{p} = 10000$ corresponding to a precipitate in an (almost) infinite-size matrix to $\tilde{p} = 200$, the attracting force of the surface increasing as $\tilde{p}$ decreases, the initial equilibrium position $\tilde{d}_{eq}$ of the dislocation at the middle of the (DA) side, obtained when the precipitate is far from the surface ($\tilde{p} = 10000$), is shifted from the middle of the (DA) side to shorter distances from the free-surface. In the case where $\tilde{h} \to 0$, i.e. for $\tilde{p} = \frac{\sqrt{2}}{2}\tilde{L} + 1 \approx 143$, it is found that a new unstable equilibrium position is obtained very close to the free-surface for $\tilde{d} \approx 3$, while the stable equilibrium position is slightly pulled back into the interface $\tilde{d}_{eq} \approx 95$ (compared to the ones obtained for higher $\tilde{p}$).

This effect for a precipitate close to the free-surface has been characterized in Figs. 3, where the position shift of the dislocation with respect to the (DA) side center $\Delta d_{eq} = d_{eq} - l/2$ has been plotted versus $\tilde{p}$ for increasing values of $\delta a/a$ from 0.005 to 0.06 with a step of 0.005 and with $\tilde{L} = 200$. For $\alpha = \pi/4$ and $\alpha = \pi/16$, it is confirmed in Figs. 3a and b that the equilibrium position shift $\Delta\tilde{d}_{eq}$ is increased as the precipitate/surface distance goes to zero, while $\Delta\tilde{d}_{eq}$

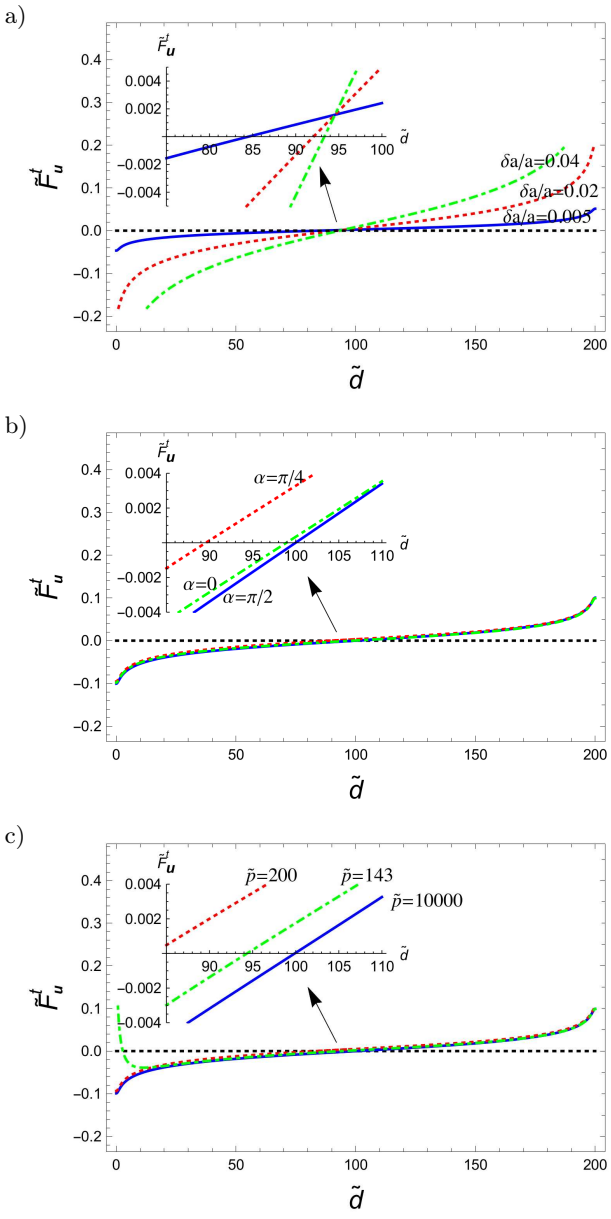

FIG. 2. Reduced total force $\tilde{F}^t_{\mathbf{u}}$ applied on the misfit dislocation in the (DA) interface versus the dimensionless distance $\tilde{d}$ of the dislocation from the corner A, with $\tilde{L} = 200$; a) different values of the misfit $\delta a/a$, with $\alpha = \pi/4$ and $\tilde{p} = 300$, b) different values of the tilt angle α, with $\delta a/a = 0.01$ and $\tilde{p} = 300$, c) different values of the precipitate/surface distance $\tilde{p}$, with $\alpha = \pi/4$ and $\delta a/a = 0.01$.

tends to zero when $\tilde{p}$ goes to infinity and the precipitate can be assumed to be embedded in an infinite-size matrix.

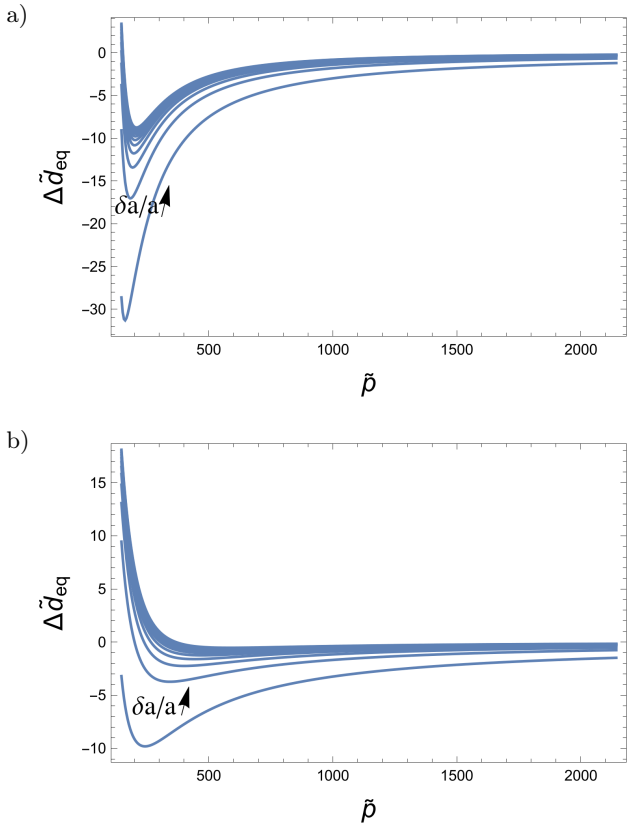

FIG. 3. Dislocation equilibrium position shift $\Delta\tilde{d}_{eq} = \tilde{d}_{eq} - l/2$ with respect to the middle of the (DA) side versus $\tilde{d}$ for increasing values of $\delta a/a$ from 0.005 to 0.06 with a step of 0.005 and with $\tilde{L} = 200$; a) $\alpha = \pi/4$, b) for $\alpha = \pi/16$.

In order to specify more precisely the effect of the misfit on the dislocation position, $\Delta\tilde{d}_{eq}$ has been then plotted versus $\delta a/a$ in Figs. 4 for two different values of the tilt angle α. Taking $\alpha = \pi/4$ in Fig. 4a, the precipitate/surface distance $\tilde{p}$ increasing from 200 to 1000, with a step of 50, it is observed that for each tested value of $\tilde{p}$, $\Delta\tilde{d}_{eq}$ increases with $\delta a/a$ and is always negative, meaning that the dislocation is closer to the surface than the middle of the (DA) side. As the precipitate/surface distance increases, the dislocation position tends to the middle of the precipitate side, as it can be expected when the precipitate is embedded in an infinite-size matrix. When the tilt angle is lower, i.e. for $\alpha = \pi/16$, it is found in Fig. 4b that for $\tilde{p}$ increasing from 200 to 350, with a step of 10, $\Delta\tilde{d}_{eq}$ still increases with $\delta a/a$ but can become positive when the precipitate is sufficiently close to the surface, i.e. for $\tilde{p} < 350$ in the present case, and when the misfit is large enough (depending on $\tilde{p}$). It can thus be stated that the combined effects

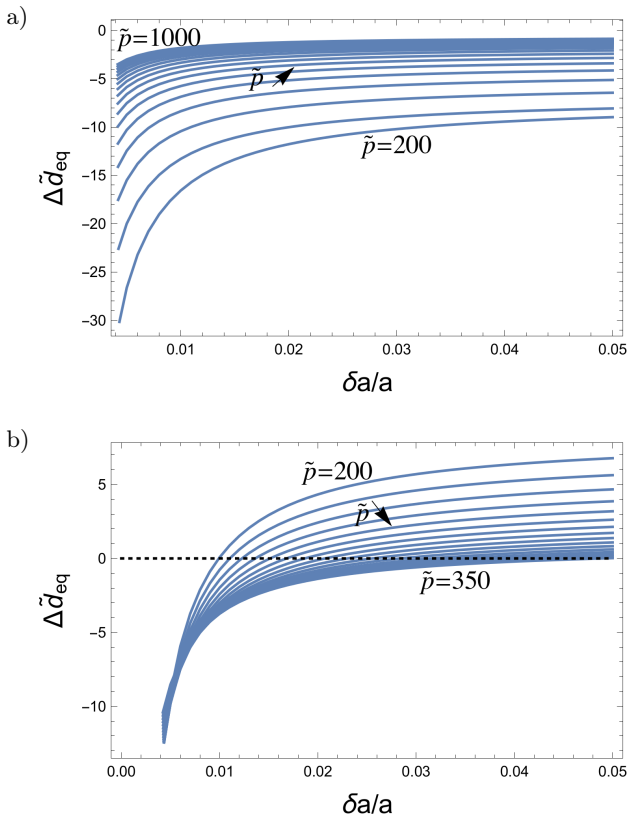

FIG. 4. Dislocation equilibrium position shift $\Delta\tilde{d}_{eq} = \tilde{d}_{eq} - l/2$ with respect to the middle of the (DA) side versus $\delta a/a$, with $\tilde{L} = 200$; a) for $\alpha = \pi/4$, the precipitate/surface distance $\tilde{p}$ increases from 200 to 1000, with a step of 50, b) for $\alpha = \pi/16$, the precipitate/surface distance $\tilde{p}$ increases from 200 to 350, with a step of 10.

of the misfit stress promoting the introduction of the dislocation into the interface and of the free-surface attracting force can lead to this shifting effect, i.e. $\Delta\tilde{d}_{eq} < 0$ for $\alpha = \pi/4$ to $\Delta\tilde{d}_{eq} > 0$ for $\alpha = \pi/16$. This effect of the tilt angle α has also been investigated in Figs. 5, where the variations of $\Delta\tilde{d}_{eq}$ versus α have been reported when $\tilde{p}$ increases from 200 to 400, with a step of 20. For $\delta a/a = 0.01$, it is observed in Fig. 5a that the misfit force can shift the equilibrium position beyond the middle of the (DA) side for low angle values and $\tilde{p} < 260$. The shifting effect is amplified in Fig. 5b when the misfit is larger, i.e. for $\delta a/a = 0.02$, the repealing effect on the dislocation into the interface being increased. In both cases of Figs. 5a and b, negative $\Delta\tilde{d}_{eq}$ increases for the larger values of α and goes to zero when $\alpha = \pi/2$ and the surface force in the gliding plane cancels (see Eq. (2.12)). To investigate the effect of the precipitate/surface distance,

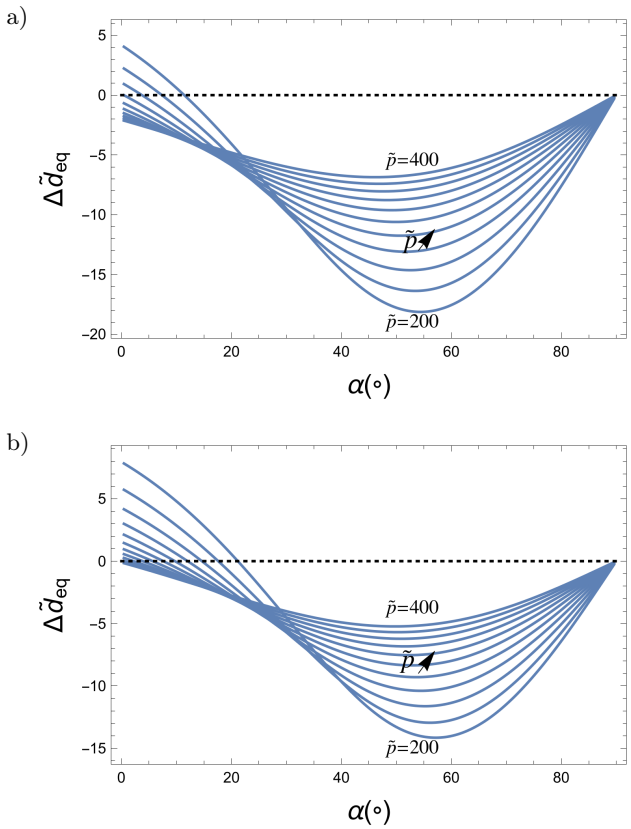

FIG. 5. Dislocation equilibrium position shift $\Delta\tilde{d}_{eq}$ with respect to the middle of the (DA) side versus tilt angle α when the precipitate/surface distance $\tilde{p}$ increases from 200 to 400, with a step of 20 and $\tilde{L} = 200$; a) $\delta a/a = 0.01$, b) $\delta a/a = 0.02$.

$\Delta\tilde{d}_{eq}$ variation versus $\tilde{p}$ has been displayed in Figs. 6 for different values of α, with $\delta a/a = 0.01$ and $\tilde{L} = 200$. It is again confirmed that $\Delta\tilde{d}_{eq}$ decreases as α increases from 0° to 55° in Fig. (6)a, while it increases in Fig. 6b when α increases from 55° to 90°. In both cases, $\Delta\tilde{d}_{eq}$ is positive for sufficiently small $\tilde{p}$ distances, becomes negative when $\tilde{p}$ increases and goes to zero when $\tilde{p}$ tends to infinity.

The size effect of the precipitate combined with α tilt angle effect has been also investigated in Fig. 7, where the relative variation of the dislocation position shift $\Delta\tilde{d}_{eq}/(\tilde{L}/2)$ has been plotted versus the precipitate side $\tilde{L}$ for different values of α, with $\tilde{p} = 200$ and $\delta a/a = 0.01$. In the particular case where the distance between the precipitate and the free-surface is fixed at $\tilde{p} = 200$, it is observed that for $\tilde{L} > 80$, the relative shift decreases as α goes from 0 to $\pi/4$. Between $\pi/4$ and $\pi/2$, the relative shift is negative for all $\tilde{L} > 10$ and goes to zero when $\alpha \to \pi/2$.

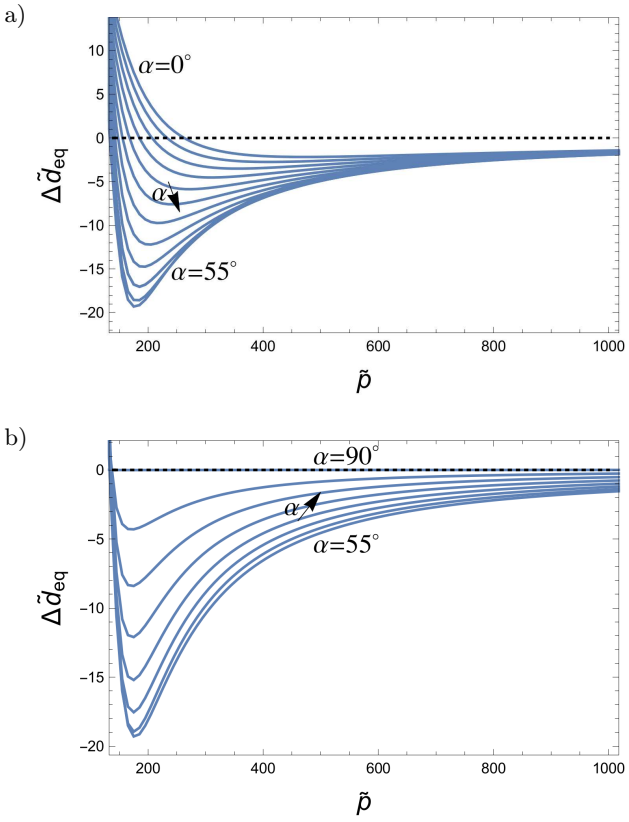

FIG. 6. Dislocation equilibrium position shift $\Delta\tilde{d}_{eq}$ with respect to the middle of the (DA) side versus the precipitate/surface distance $\tilde{p}$, with $\delta a/a = 0.01$ and $\tilde{L} = 200$; a) the tilt angle α increases from 0° to 55°, with a step of 5°, b) the tilt angle α increases from 55° to 90°, with a step of 5°.

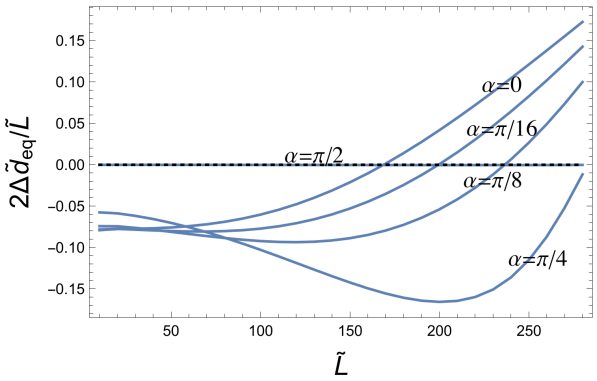

FIG. 7. Relative equilibrium position shift $2\Delta\tilde{d}_{eq}/\tilde{L}$ versus the precipitate side $\tilde{L}$ for different values of the α tilt angle, with $\tilde{p} = 200$ and $\delta a/a = 0.01$.

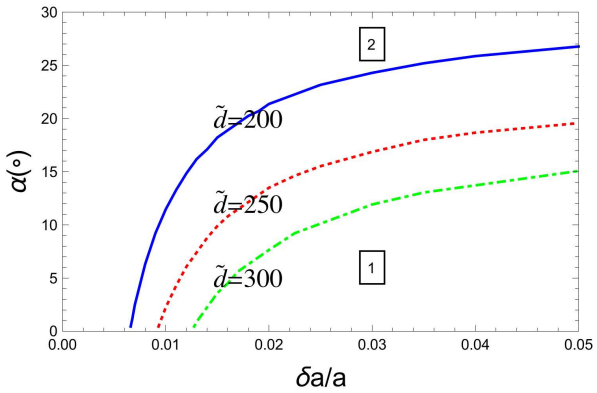

FIG. 8. Position diagram in the $(\delta a/a, \alpha)$ plane of the misfit edge dislocation for different values of $\tilde{d}$, with $\tilde{L} = 200$. In region 1, the dislocation is closer to the matrix free-surface than the middle of the (DA) side. In region 2, the dislocation is farther to the surface than the middle of the (DA) side.

Finally, a "position diagram" for the misfit dislocation has been plotted in Fig. 8 in the $(\delta a/a, \alpha)$ plane for different values of $\tilde{p}$, with $0 \leq \alpha \leq \pi/2$ and $\tilde{L} = 200$. Each curve at given $\tilde{d}$ delimits two regions in the plane. In region 1, the equilibrium position of the dislocation is closer to the surface than the middle of the (DA) side. In region 2, the dislocation is located farther than the middle of the (DA) side. The main feature of this evolution is that as the misfit $\delta a/a$ increases, the critical angle α characterizing this shifting effect increases.

3. Conclusion

The equilibrium position of a misfit edge dislocation has been theoretically determined in the interface of a square shaped precipitate embedded in a semi-infinite matrix, when the precipitate is tilted relative to the matrix free-surface. From the study of the variations of the force applying on the dislocation, the combined effects of the precipitate tilt angle, misfit strain and precipitate/free-surface distance have been analyzed on the dislocation equilibrium position. It has been first found that due to misfit strain, a stable equilibrium position of the dislocation may exit into the precipitate/matrix interfaces. This equilibrium position has been then found to be shifted to shorter values with respect to the middle of the precipitate side as the corresponding interface is tilted relative to the free-surface from the configuration where it is the perpendicular to the free-surface. This effect is enhanced as the precipitate/free-surface distance is reduced. The next step of this study would be to investigate at the microscopic scale, using molecular dynamics simulations for example, the nucleation mechanisms to determine where the misfit dislocation can be created as well as the energy barrier and energy gain resulting from this formation.

4. Appendix

For the side (AB), taking $b_x^v = -b_M \cos\alpha$ and $b_y^v = b_M \sin\alpha$, the Airy's function $\phi_M^{(AB)}$ is given by:

$$\phi_M^{(AB)}(x,y) = \int_0^{l\cos\alpha} \phi_{\mathbf{b}_v}(x, x_v, y, -x_v \tan\alpha - h)\, \frac{dx_v}{a\cos\alpha}. \tag{4.1}$$

It yields:

$$\begin{aligned}\phi_M^{(AB)}(x,y) = {} & \frac{\mu\delta a}{2\pi(1-\nu)a} \\ & \times \big(f_1(0,-h) - f_1(l\cos\alpha,-h) + f_2(0,-h) - f_2(l\cos\alpha,-h)\big).\end{aligned} \tag{4.2}$$

For the side (DC), taking $b_x^v = b_M \cos\alpha$ and $b_y^v = -b_M \sin\alpha$, the Airy's function $\phi_M^{(DC)}$ is given by:

$$\phi_M^{(DC)}(x,y) = \int_{-l\sin\alpha}^{l(\cos\alpha-\sin\alpha)} \phi_{\mathbf{b}_v}(x, x_v, y, -x_v \tan\alpha - h - l/\cos\alpha)\, \frac{dx_v}{a\cos\alpha}. \tag{4.3}$$

It yields:

$$\begin{aligned}\phi_M^{(DC)}(x,y) = {} & \frac{\mu\delta a}{2\pi(1-\nu)a} \\ & \times \big(f_1(l(\cos\alpha-\sin\alpha),-h-l/\cos\alpha) - f_1(-l\sin\alpha,-h-l/\cos\alpha) \\ & + f_2(l(\cos\alpha-\sin\alpha),-h-l/\cos\alpha) - f_2(-l\sin\alpha,-h-l/\cos\alpha)\big).\end{aligned} \tag{4.4}$$

For the side (CB), taking $b_x^v = b_M \sin\alpha$ and $b_y^v = b_M \cos\alpha$, the Airy's function $\phi_M^{(CB)}$ is given by:

$$\phi_M^{(CB)}(x,y) = \int_{l(\cos\alpha-\sin\alpha)}^{l\cos\alpha} \phi_{\mathbf{b}_v}(x, x_v, y, x_v/\tan\alpha - h - l/\sin\alpha)\, \frac{dx_v}{a\sin\alpha}. \tag{4.5}$$

It yields:

$$\begin{aligned}\phi_M^{(CB)}(x,y) = {} & \frac{\mu\delta a}{2\pi(1-\nu)a} \\ & \times \big(g_1(l\cos\alpha,-h-l/\sin\alpha) - g_1(l(\cos\alpha-\sin\alpha),-h-l/\sin\alpha) \\ & + g_2(l\cos\alpha,-h-l/\sin\alpha) - g_2(l(\cos\alpha-\sin\alpha),-h-l/\sin\alpha)\big).\end{aligned} \tag{4.6}$$

For the side (DA), taking $b_x^v = -b_M \sin\alpha$ and $b_y^v = -b_M \cos\alpha$, the Airy's function $\phi_M^{(DA)}$ is given by:

$$\phi_M^{(DA)}(x,y) = \int_{-l\sin\alpha}^{0} \phi_{\mathbf{b}_v}(x, x_v, y, x_v/\tan\alpha - h)\,\frac{dx_v}{a\sin\alpha}. \tag{4.7}$$

It yields:

$$\begin{aligned}\phi_M^{(DA)}(x,y) = {} & \frac{\mu\delta a}{2\pi(1-\nu)a}\big(g_1(-l\sin\alpha,-h) - g_1(0,-h) \\ & + g_2(-l\sin\alpha,-h) - g_2(0,-h)\big).\end{aligned} \tag{4.8}$$

The functions f_1, f_2, g_1 and g_2 are defined as:

$$\begin{aligned}& f_1(x_v,y_c) \\ &= \frac{1}{4}\Bigg(2x_v^2\tan\alpha\ln\big[-2x_v(\tan\alpha(y+y_c)+x) + x_v^2\sec^2\alpha + x^2 + (y+y_c)^2\big] \\ &\quad + 4y_c\big(\cos^2\alpha(\tan\alpha(y+y_c)+x) \\ &\quad \times \ln\Big(-2x_v(\tan\alpha(y+y_c)+x) + x_v^2\sec^2\alpha + x^2 + (y+y_c)^2\Big) \\ &\quad + 2\cos^2\alpha(-x\tan\alpha + y + y_c) \\ &\quad \times \tan^{-1}\left[\frac{-x_v\sec^2\alpha + \tan\alpha(y+y_c) + x}{-x\tan\alpha + y + y_c}\right] + 2x_v\Bigg) \\ &\quad + \cos 2\alpha\cos^2\alpha\cot\alpha(-x\tan\alpha + y + y_c)^2 \\ &\quad \times \ln\big[-2x_v(\tan\alpha(y+y_c)+x) + x_v^2\sec^2\alpha + x^2 + (y+y_c)^2\big] \\ &\quad - 4y\sin\alpha\cos\alpha(-x\sin 2\alpha + \cos 2\alpha(y+y_c) + y_c) \\ &\quad \times \ln\big[-2x_v(\tan\alpha(y+y_c)+x) + x_v^2\sec^2\alpha + x^2 + (y+y_c)^2\big] \\ &\quad - 2\sin\alpha\cos\alpha\big(\cos 2\alpha\big(x^2 - (y+y_c)^2\big) + 2x\sin 2\alpha(y+y_c)\big) \\ &\quad \times \ln\big[-2x_v(\tan\alpha(y+y_c)+x) + x_v^2\sec^2\alpha + x^2 + (y+y_c)^2\big] \\ &\quad + \sin\alpha\cos 2\alpha\cos\alpha(\cot\alpha(y-y_c)+x)^2 \\ &\quad \times \ln\big[x_v^2\sec^2\alpha + 2x_v\tan\alpha(y-y_c) + x(x-2x_v) + (y-y_c)^2\big] \\ &\quad - 4x_v y_c\ln\big[(-x_v\tan\alpha + y + y_c)^2 + (x-x_v)^2\big] \\ &\quad - 4x_v\sin\alpha(x\cos\alpha + \sin\alpha(y+y_c)) \\ &\quad - 4\cos^4\alpha(-x\tan\alpha + y + y_c)^2\tan^{-1}\left[\frac{-x_v\sec^2\alpha + \tan\alpha(y+y_c) + x}{-x\tan\alpha + y + y_c}\right] \\ &\quad + 4\cos^4\alpha(x\tan\alpha + y - y_c)^2\tan^{-1}\left[\frac{-x_v\sec^2\alpha + \tan\alpha(y_c - y) + x}{x\tan\alpha + y - y_c}\right]\end{aligned} \tag{4.9}$$

$$
\begin{aligned}
&- 8y\cos^4\alpha\big(x\tan^3\alpha - x\tan\alpha - \tan^2\alpha(2y+y_c) + y_c\big)\\
&\times \tan^{-1}\left[\frac{-x_v\sec^2\alpha + \tan\alpha(y+y_c) + x}{-x\tan\alpha + y + y_c}\right]\\
&- \cot\alpha(-x_v\tan\alpha + y + y_c)^2\ln\big[(-x_v\tan\alpha + y + y_c)^2 + (x-x_v)^2\big]\\
&- \cot\alpha(x_v\tan\alpha + y - y_c)^2\ln\big[(x_v\tan\alpha + y - y_c)^2 + (x-x_v)^2\big]\\
&- 8\sin\alpha\cos\alpha(\cos\alpha(y+y_c)\\
&- x\sin\alpha)(x\cos\alpha + \sin\alpha(y+y_c))\tan^{-1}\left[\frac{-x_v\sec^2\alpha + \tan\alpha(y+y_c) + x}{-x\tan\alpha + y + y_c}\right]\\
&+ 2xx_v\sin 2\alpha - x_v\cos 2\alpha(y+y_c)\\
&+ x_v(\cos 2\alpha + 3)(y-y_c) + 8x_v y\sin^2\alpha - 3x_v(y+y_c)\Big),
\end{aligned}
$$

$$
\begin{aligned}
(4.10)\qquad f_2(x_v,y_c) = \frac{1}{8}\tan\alpha\Big(&\cos\alpha\big(\cos\alpha\big(-\big(3x^2+5y^2-2yy_c+y_c^2\big)\big)\\
&+\cos 3\alpha\big(x^2+(3y-y_c)(y+y_c)\big)\\
&+2x(\sin\alpha-\sin 3\alpha)(y-y_c)\big)\ln\big[\cos 2\alpha\big(x^2-2xx_v+(y+y_c)^2\big]\\
&-2x_v\sin 2\alpha(y+y_c)+x^2-2xx_v+2x_v^2+(y+y_c)^2\big)\\
&+\cos\alpha\big(\cos\alpha\big(3x^2+(y-y_c)^2\big)+\cos 3\alpha\big((y-y_c)^2-x^2\big)\\
&+2x(\sin 3\alpha-\sin\alpha)(y-y_c)\big)\ln\big[\cos 2\alpha\big(x^2-2xx_v+(y-y_c)^2\big)+2x_v\sin 2\alpha(y-y_c)\\
&+x^2-2xx_v+2x_v^2+(y-y_c)^2\big]+2\sin 2\alpha\big(-\cos 2\alpha\big(x^2+(3y-y_c)(y+y_c)\big)\\
&+2x\sin 2\alpha(y-y_c)+x^2+(y-y_c)^2\big)\cot^{-1}\left[\frac{2\cos\alpha(\cos\alpha(y+y_c)-x\sin\alpha)}{x\cos 2\alpha+\sin 2\alpha(y+y_c)+x-2x_v}\right]\\
&-2x_v(x_v-2x)\ln\big[(-x_v\tan\alpha+y+y_c)^2+(x-x_v)^2\big]\\
&+2x_v(x_v-2x)\ln\big[(x_v\tan\alpha+y-y_c)^2+(x-x_v)^2\big]\\
&+8\sin\alpha\cos\alpha(x\sin\alpha+\cos\alpha(y-y_c))^2\\
&\times\cot^{-1}\left[\frac{2\cos\alpha(x\sin\alpha+\cos\alpha(y-y_c))}{x\cos 2\alpha+\sin 2\alpha(y_c-y)+x-2x_v}\right]-4x_vy\sin 2\alpha\Big),
\end{aligned}
$$

$$
\begin{aligned}
(4.11)\qquad &g_1(x_v,y_c)\\
&=\frac{1}{4}\Big(\sin 2\alpha\big((y-y_c)^2\ln\big[-2x_v(\cot\alpha(y-y_c)+x)+x_v^2\csc^2\alpha+x^2+(y-y_c)^2\big]\\
&+\big(y^2+2yy_c-y_c^2\big)\ln\big[x_v^2\csc^2\alpha+2x_v\cot\alpha(y+y_c)+x(x-2x_v)+(y+y_c)^2\big)\big]\\
&-\frac{1}{4}\sin 4\alpha\big(\big(x^2+(3y-y_c)(y+y_c)\big)\\
&\times\ln\big[x_v^2\csc^2\alpha+2x_v\cot\alpha(y+y_c)+x(x-2x_v)+(y+y_c)^2\big]\\
&-(x+y-y_c)(x-y+y_c)
\end{aligned}
$$

$$
\begin{aligned}
&\times \ln\big[-2x_v(\cot\alpha(y-y_c)+x)+x_v^2\csc^2\alpha+x^2+(y-y_c)^2\big)\big]\\
&+\cos 2\alpha\big(2x\sin^2\alpha(y_c-y)\\
&\times \ln\big[-2x_v(\cot\alpha(y-y_c)+x)+x_v^2\csc^2\alpha+x^2+(y-y_c)^2\big]\\
&+x(y-y_c)\ln\big[x_v^2\csc^2\alpha+2x_v\cot\alpha(y+y_c)+x(x-2x_v)+(y+y_c)^2\big]+2x_vy\big)\\
&+2\sin^2\alpha\big(\cos 2\alpha\big(x^2+(3y-y_c)(y+y_c)\big)+2x\sin 2\alpha(y_c-y)\\
&+x^2+(y-y_c)^2\big)\tan^{-1}\left[\frac{-x_v\csc^2\alpha-\cot\alpha(y+y_c)+x}{x\cot\alpha+y+y_c}\right]\\
&-\big(x\cos^2 2\alpha(y-y_c)+2x_v^2\cot\alpha\big)\\
&\times\ln\big[x_v^2\csc^2\alpha+2x_v\cot\alpha(y+y_c)+x(x-2x_v)+(y+y_c)^2\big]\\
&+2x_v\big((y_c-y)\ln\big[(x_v\cot\alpha-y+y_c)^2+(x-x_v)^2\big]+y\big)\\
&+x_v\big(x_v\cot\alpha\ln\big[(x_v\cot\alpha-y+y_c)^2+(x-x_v)^2\big]\\
&+(x_v\cot\alpha+2y-2y_c)\ln\big[(x_v\cot\alpha+y+y_c)^2+(x-x_v)^2\big]\big)\\
&+4\sin^2\alpha(x\cos\alpha+\sin\alpha(y_c-y))^2\tan^{-1}\left[\frac{-x_v\csc^2\alpha+\cot\alpha(y-y_c)+x}{-x\cot\alpha+y-y_c}\right]\Big),
\end{aligned}
\tag{4.12}
$$

$$
\begin{aligned}
&g_2(x_v,y_c)\\
&=-\frac{1}{4}\cot\alpha\Big(-\sin\alpha\big(\sin\alpha\big(\cos 2\alpha\big(x^2+(3y-y_c)(y+y_c)\big)+2\big(x^2+2y^2\big)\big)\\
&+x\cos\alpha(y-y_c)+x\cos 3\alpha(y-y_c)\big)\\
&\times\ln\big[-\cos 2\alpha\big(x^2-2xx_v+(y+y_c)^2\big)+2x_v\sin 2\alpha(y+y_c)\\
&+x^2-2xx_v+2x_v^2+(y+y_c)^2\big]\\
&+\sin\alpha\big(\sin\alpha\big(\cos 2\alpha(x+y-y_c)(x-y+y_c)+2x^2\big)+x\cos\alpha(y-y_c)\\
&+x\cos 3\alpha(y-y_c)\big)\ln\big(-\cos 2\alpha\big(x^2-2xx_v+(y-y_c)^2\big)\\
&+2x_v\sin 2\alpha(y_c-y)+x^2-2xx_v+2x_v^2+(y-y_c)^2\big)\\
&+\sin 2\alpha\big(\cos 2\alpha\big(x^2+(3y-y_c)(y+y_c)\big)+2x\sin 2\alpha(y_c-y)+x^2\\
&+(y-y_c)^2\big)\cot^{-1}\left[\frac{2\sin\alpha(x\cos\alpha+\sin\alpha(y+y_c))}{x\cos 2\alpha+\sin 2\alpha(y+y_c)-x+2x_v}\right]\\
&+x_v(x_v-2x)\ln\big[(x_v\cot\alpha-y+y_c)^2+(x-x_v)^2\big]-x_v(x_v-2x)\\
&\times\ln\big[(x_v\cot\alpha+y+y_c)^2+(x-x_v)^2\big]\\
&-4\sin\alpha\cos\alpha(x\cos\alpha+\sin\alpha(y_c-y))^2\\
&\times\cot^{-1}\left[\frac{2\sin\alpha(x\cos\alpha+\sin\alpha(y_c-y))}{x\cos 2\alpha+\sin 2\alpha(y_c-y)-x+2x_v}\right]+2x_vy\sin 2\alpha\Big).
\end{aligned}
\tag{4.13}
$$

Finally, the Airy's function characterizing the misfit stress $\bar{\bar{\sigma}}_M$ is found to be:

$$
\phi_M(x,y)=\phi_M^{(CB)}(x,y)+\phi_M^{(DA)}(x,y)+\phi_M^{(DC)}(x,y)+\phi_M^{(AB)}(x,y),
\tag{4.14}
$$

and the stress components are derived as [30]:

$$\begin{aligned}\sigma_{xx}^{M}(x,y) &= \frac{\partial^2}{\partial y^2}\phi_M(x,y),\\ \sigma_{xy}^{M}(x,y) &= -\frac{\partial^2}{\partial x \partial y}\phi_M(x,y),\\ \sigma_{yy}^{M}(x,y) &= \frac{\partial^2}{\partial x^2}\phi_M(x,y).\end{aligned} \tag{4.14}$$

References

1. B. LIU, D. RAABE, F. ROTERS, A. ARSENLIS, *Interfacial dislocation motion and interactions in single-crystal superalloys*, Acta Materialia, **79**, 216–233, 2014.
2. T. CHENK, R. TREHOREL, L. DIRAND, A. JACQUES, *Dislocation densities and velocities within the γ channels of an SX superalloy during in situ high-temperature creep tests*, Materials, **11**, 1527, 2018.
3. S.M. HAFEZ HAGHIGHAT, G. EGGELER, D. RAABE, *Effect of climb on dislocation mechanisms and creep rates in γ'-strengthened Ni base superalloy single crystals: a discrete dislocation dynamics study*, Acta Materialia, **61**, 3709–3723, 2013.
4. M. PROBST-HEIN, A. DLOUHY, G. EGGELER, *Interface dislocations in superalloy single crystals*, Acta Materialia, **47**, 8, 2497–2510, 1999.
5. S.S. QUEK, Y. XIANG, D.J. SROLOVITZ, *Loss of interface coherency around a misfitting spherical inclusion*, Acta Materialia, **59**, 14, 5398–5410, 2011.
6. J. XIONG, Y. ZHU, Z. LI, M. HUANG, *Quantitative study on interactions between interfacial misfit dislocation networks and matrix dislocations in Ni-based single crystal superalloys*, Acta Mechanica Solida Sinica, **30**, 345–353, 2017.
7. S. RAYCHAUDHURI, E.T. YU, *Critical dimensions in coherently strained coaxial nanowire heterostructures*, Journal of Applied Physics, **99**, 114308, 2006.
8. H. AHMADZADEH-BAKHSHAYESH, M.YU. GUTKIN, H.M. SHODJA, *Surface/interface effects on elastic behavior of a screw dislocation in an eccentric core-shell nanowire*, International Journal of Solid and Structures, **49**, 1665–1675, 2012.
9. Q.H. FANG, J.H. CHEN, P.H. WEN, Y.W. LIU, *Misfit dislocations in an annular strained film grown on a cylindrical nanopore surface*, Scripta Materialia, **60**, 6, 395–398, 2009.
10. X. WANG, E. PAN, A.K. ROY, *New phenomena concerning a screw dislocation interacting with two imperfect interfaces*, Journal of the Mechanics and Physics, **55**, 2717–2734, 2007.
11. K.E. AIFANTIS, A.L. KOLESNIKOVA, A.E. ROMANOV, *Nucleation of misfit dislocations and plastic deformation in core/shell nanowires*, Philosophical Magazine, **87**, 4731–4757, 2007.
12. M.YU. GUTKIN, K.V. KUZMIN, A.G. SHEINERMAN, *Misfit stresses and relaxation mechanisms in a nanowire containing a coaxial cylindrical inclusion of finite height*, Physica Status Solidi (b), **248**, 1651–1657, 2011.
13. M.YU. GUTKIN, I.A. OVIDKO, A.G. SHEINERMAN, *Misfit dislocations in wire composite solids*, Journal of Physics: Condensed Matter, **12**, 25, 5391–5401, 2000.

14. I.A. OVIDKO, A.G.K. SHEINERMAN, *Misfit dislocation loops in composite nanowires*, Philosophical Magazine, **84**, 2103–2118, 2004.

15. M.YU. GUTKIN, A.L. KOLESNIKOVA, S.A. KRASNITCKII, A.E. ROMANOV, *Misfit dislocation loops in composite core-shell nanoparticles*, Physics of the Solid State, **56**, 723–730, 2014.

16. M.YU. KRAUCHANKA, S.A. KRASNITCKII, M.YU. GUTKIN, A.L. KOLESNIKOVA, A.E. ROMANOV, *Circular loops of misfit dislocations in decahedral core-shell nanoparticles*, Scripta Materialia, **167**, 81–85, 2019.

17. M.YU. GUTKIN, A.L. KOLESNIKOVA, S.A. KRASNITCKII, A.E. ROMANOV, A.G. SHALKOVSKII, *Misfit dislocation loops in hollow core-shell nanoparticles*, Scripta Materialia, **83**, 1–4, 2014.

18. M.YU. GUTKIN, S. REZAZADEH KALEHBASTI, H.M. SHODJA, *Surface/interface effects on elastic behavior of an edge dislocation in the shell of a core-shell nanowire*, European Journal of Mechanics - A/Solids, **41**, 86–100, 2013.

19. M.YU. GUTKIN, C. ENZEVAEE, H.M. SHODJA, *Interface effects on elastic behavior of an edge dislocation in a core-shell nanowire embedded to an infinite matrix*, International Journal of Solids and Structures, **50**, 1177–1186, 2013.

20. C. ENZEVAEE, M.YU. GUTKIN, H.M. SHODJA, *Surface/interface effects on the formation of misfit dislocation in a core-shell nanowire*, Philosophical Magazine, **94**, 492–519, 2014.

21. S.S. MOEINI-ARDAKANI, M.YU. GUTKIN, H.M. SHODJA, *Elastic behavior of an edge dislocation inside the wall of a nanotube*, Scripta Materialia, **64**, 709–712, 2011.

22. H.M. SHODJA, M.YU. GUTKIN, S.S. MOEINI-ARDAKANI, *Effect of surface stresses on elastic behavior of a screw dislocation inside the wall of a nanotube*, Physica Status Solidi (b), **248**, 1437–1441, 2011.

23. M.YU. GUTKIN, I.A. OVIDKO, I.A.G. SHEINERMAN, *Misfit dislocations in composites with nanowires*, Journal of Physics: Condensed Matter, **15**, 3539–3554. 2003.

24. K.N. MIKAELYAN, M.YU. GUTKIN, E.N. BORODIN, A.E. ROMANOV, *Dislocation emission from the edge of a misfitting nanowire embedded in a free-standing nanolayer*, International Journal of Solid and Structures, **161**, 127–135, 2019.

25. J. COLIN, *Dislocation formation from the free-surface of a two-phase solid*, Mechanics of Materials, **137**, 103094, 2019.

26. X. ZHAO, R. DUDDU, S.P.A. BORDAS, J. QU, *Effects of elastic strain energy and interfacial stress on the equilibrium morphology of misfit particles in heterogeneous solids*, Journal of the Mechanics and Physics of Solids, **61**, 1433–1445, 2013.

27. T. MURA, *Micromechanics of Defects in Solids*, Martinus Nijhoff Publishers, Dordrecht, The Netherlands, 1987.

28. J.P. HIRTH, J. LOTH, *Theory of Dislocations*, John Wiley & Sons, Wiley Interscience Publication, 1982.

29. J.W. JAGANNADHAM, M.J. MARCINKOWSKI, *Comparison of the image and surface dislocation models*, Physica Status Solidi (a), **50**, 293–302, 1978.

30. S. TIMOSHENKO, J.N. GOODIER, *Theory of Elasticity*, Mc Graw-Hill Book Company, Inc., New York, USA, 1951.

31. M. PEACH, M.J.S. KÖHLER, *The forces exerted on dislocations and the stress fields produced by them*, Physical Review, **80**, 3, 436–439, 1950.

Received June 10, 2020; revised version August 25, 2020.
Published online October 7, 2020.